SCIENCE CHINA
Technological Sciences

•Article•

September 2023 Vol.66 No.9: 2561–2574
https://doi.org/10.1007/s11431-022-2393-2

Exploring impact of street layout on urban flood risk of people and vehicles under extreme rainfall based on numerical experiments

MEI Chao[1,2,3], LIU JiaHong[1,2*], SHI HongYuan[1], WANG Hao[1,2], WANG Jia[1,2], DONG LiRong[1], SONG TianXu[1] & ZHANG HaiJia[1]

[1] *State Key Laboratory of Simulation and Regulation of Water Cycle in River Basin, China Institute of Water Resources and Hydropower Research, Beijing 100038, China;*
[2] *Key Laboratory of River Basin Digital Twinning of Ministry of Water Resources (Preparation), Beijing 100038, China;*
[3] *Beijing Key Laboratory of Urban Water Cycle and Sponge City Technology, Beijing Normal University, Beijing 100875, China*

Received December 14, 2022; accepted April 4, 2023; published online August 21, 2023

Urban street layout is an important factor in the formation process, characteristics, and risk level of urban flooding; therefore, this study numerically investigates the impact of street layout on urban flood risk to people and vehicles. Four typical street-layout scenarios with areas of 3 km × 3 km are established based on a block-scale investigation. The layout types are regular grid, irregular grid, radial, and annular. Urban inundation models are then constructed for these typical street layouts based on the two-dimensional (2D) hydrodynamic method. Two historic, extreme rainfall events, which occurred in Beijing on July 21, 2012 and in Zhengzhou on July 20, 2021, are used as rainstorm scenarios for urban inundation modelling. The flood risks to people and vehicles are then calculated. Results show that, for an extreme rainstorm on the block scale, the street layout impacts the spatial and temporal distributions of the inundation variables, which include the water depth, flow velocity, flood volume, and inundated area. Moreover, for the same extreme-rainfall scenario, the greatest differences in the total flood volume, maximum street-water depth, and maximum street-flow velocity caused by street-layout differences are 17.22%, 60.25%, and 61.50%, respectively. Among the four street layouts considered in this study, the annular street layout exhibits the lowest degrees of inundation and flood risk. For the same extreme-rainfall scenario, the proportions of high-risk road sections for adults and children in this layout are 58.89% and 62.28% smaller than those for the layout with the largest proportion of high-risk road sections, respectively; the proportions of high-risk road sections for the Honda Accord and Audi Q7 were 55.31% and 53.04% smaller, respectively. The findings of this study may aid scientific understanding and development of "flood-sensitive" block-scale street layouts and urban planning in the context of the changing environment.

urban inundation, street layout, urban form, flood risk, hydrodynamic simulation

Citation: Mei C, Liu J H, Shi H Y, et al. Exploring impact of street layout on urban flood risk of people and vehicles under extreme rainfall based on numerical experiments. Sci China Tech Sci, 2023, 66: 2561–2574, https://doi.org/10.1007/s11431-022-2393-2

1 Introduction

In recent decades, the harm to people as well as damage to economies and societies worldwide due to urban flooding has been increasing continuously [1–3]. Urban flood risk is increasing in many areas owing to global climate change and rapid urbanization [4–6]. In all flood-prone areas, the urban street network is the major area affected by inundations, and these inundations pose serious threats to people and vehicles [7,8]. Therefore, research on flood risk modelling and management of urban streets has become an important issue in the field of urban flooding [9,10].

Various types of losses may be caused by urban flooding, including direct damage and indirect losses; however, the

*Corresponding author (email: liujh@iwhr.com)

loss of human life is the most severe type of loss [11,12]. Many studies have shown that, in urban flood disasters, many casualties occur on urban roads. Incidents include people drowning in a flooded road as well as people suffocating due to being trapped in vehicles washed away in the flood [13]. For example, on July 20, 2021, an extreme rainstorm and flooding occurred in Zhengzhou, and some fatalities resulted from people wading in road culverts [14]. Similar incidents have been reported in Germany, the United States, and many countries in Southeast Asia, thereby indicating that road casualties caused by urban flooding under extreme rainstorms is a common global problem [15,16]. Therefore, the risk of urban-road flooding under extreme rainstorm scenarios requires more attention [17,18].

Many factors cause urban flooding; however, most recent research in this field has focused on extreme rainfall and impervious areas as well as the lack of green infrastructure and drainage systems [19,20]. In the past 20 years, in-depth studies have examined these aspects, and the results have been instrumental in improving the scientific understanding of urban flooding mechanisms. Further researched has refined our perspective on these influencing factors; thus, the effects of urban artificial buildings and microtopographies on urban flooding have attracted greater attention [21]. Many studies have considered the influence of the spatial pattern of the underlying urban surface on the inundation features [22]. In particular, Bruwier et al. [21] analyzed the influence of urban forms on surface flow in urban pluvial flooding based on the two-dimensional (2D) hydrodynamic modelling of 2000 synthetic urban forms; their results showed that urban forms strongly impact urban flooding. Similarly, Wang et al. [23] explored the spatial characteristics and driving factors of urban flooding in Chinese megacities, and Papilloud and Keiler [17] evaluated patterns in road-network vulnerability to extreme floods based on accessibility measures. Mignot et al. [24] analyzed the effects of obstacles located in streets and on façades, and they confirmed that those in streets affected the flood process significantly. Li et al. [22] studied the influence of urban forms on long-duration urban flooding via experiments and computational analysis. Lu et al. [25] reviewed flood-induced transport disruptions on urban streets and roads in Chinese megacities and discussed the resultant lessons and future agendas. Dong et al. [8] conducted experimental and numerical model-based studies on flash-flood inundation processes for a typical urban street. Finally, Zhou et al. [26] analyzed the effects of building configurations on urban stormwater management on the block scale using the XGBoost framework. The findings of the above studies indicated that urban forms, such as street layouts and building arrangements, significantly affect urban-flood formation processes and inundation characteristics; thus, they influence the resultant flood risk to people and vehicles.

Based on current studies on the influence of urban form on flooding, flood-sensitive and flood-resilient urban planning may be more economical than upgrading existing flood-defense and urban drainage-system infrastructures [27,28]. To date, more studies have been conducted on the effects of urban-building and impervious-area spatial arrangements on urban inundations compared with those on street floods that directly threaten human and vehicle safety. However, to scientifically manage urban-street flood risks, it is important to first understand how street flooding occurs and to identify the influencing factors that affect the risk related to people and vehicles. Urban street is an important factor in both the formation process and final state of the urban form. Under extreme rainstorm conditions, the drainage system is typically overloaded, and urban streets often act as flood pathways and channels for surface inundation. Therefore, street layouts significantly impact urban inundation and flood risk, and flood-sensitive urban-street design is an integral aspect of urban flood risk management under extreme rainfall scenarios [23,29]. Thus, research to further optimize flood risk management under extreme rainstorms and reduce casualties is greatly needed.

Previous studies on road networks have focused on their functions and have considered topics such as traffic efficiency and pedestrian crashes. However, these studies have paid little attention to the impact of urban roads on flood risk, and especially on the risk to people and vehicles [30]. In recent years, an increasing number of studies have investigated the effects of street layouts and street networks on urban-form elasticity. Notably, Yang et al. [31] conducted a case study of a stormwater drainage-building-road transport nexus in the context of urban flooding. Moreover, Bernardini et al. [9] analyzed the influence of urban-layout pedestrian-evacuation behaviors on flood risk assessments for riverine historic built environments. These studies provided a foundation for exploring the influence of street layout on urban flooding.

The objective of the present study is to explore the influence of street layout on urban flood risk to people and vehicles under extreme rainfall conditions based on the above studies. Numerical experiments are conducted based on an urban inundation hydrodynamic simulation for typical street layouts under extreme rainfall. We combine actual observations and the results of international studies to investigate the spatial distributions of urban streets on the regional scale and construct typical scenarios. Numerical experiments are then conducted to provide a scientific basis for flood-sensitive urban street design and flood risk management. Note that the street layouts considered in this study are idealized virtual scenarios produced by software simulations, which enabled objective and diverse simulation results. This approach is employed to eliminate the interference of different variable factors and better focus on

the influence of street layout on the inundation process. The flood simulation is developed with the widely used 2D hydrodynamic simulation method [22,23], which is recognized as a feasible and economical research method. In addition, this study focuses on variables that indicate the severity of the flood itself (that is, the water depth) as well as on the flood risk to people and vehicles. The latter are calculated using the instability formula, based on the flood-simulation results.

2 Methodology

2.1 Flood simulation and risk assessment

2.1.1 Urban flood simulation

The TELEMAC-2D module, which is a 2D hydrodynamic module developed by the National Laboratory of Hydraulics and Environment, France [32,33], was used to conduct the urban inundation simulation in this study. TELEMAC-2D mainly simulates 2D free surface flows by solving 2D Saint-Venant equations; the calculation is based on a highly adaptable unstructured triangular grid [34]. Li et al. [19] previously verified the applicability of TELEMAC-2D to urban inundation simulations via an analysis of classical examples.

TELEMAC-2D utilizes the non-conservation form of the 2D shallow-water equation, including the continuity and momentum equations [32]:

$$\frac{\partial h}{\partial t}+\frac{\partial (hu)}{\partial x}+\frac{\partial (hv)}{\partial y}=Sce, \tag{1}$$

$$\frac{\partial u}{\partial t}+u\frac{\partial u}{\partial x}+v\frac{\partial u}{\partial y}=-g\frac{\partial Z}{\partial x}+F_x+v_e\left(\frac{\partial^2 u}{\partial x^2}+\frac{\partial^2 u}{\partial y^2}\right), \tag{2}$$

$$\frac{\partial v}{\partial t}+u\frac{\partial v}{\partial x}+v\frac{\partial v}{\partial y}=-g\frac{\partial Z}{\partial y}+F_y+v_e\left(\frac{\partial^2 v}{\partial x^2}+\frac{\partial^2 v}{\partial y^2}\right), \tag{3}$$

where u and v are the flow rates in the x and y directions, respectively, m/s; h is the water depth, m; t is time, s; Sce is the fluid source or sink, m/s; Z is the free surface elevation, m; v_e is the effective viscosity coefficient, m^2/s; g is the acceleration of gravity, m/s^2; and F_x and F_y are the friction terms in the x- and y-directions, respectively [32].

When the TELEMAC-2D module was used to conduct rainfall-runoff modelling, the infiltration simulation was based on the Soil Conservation Service-curve number (SCS-CN) method, in which the *CN* coefficient was used to describe the infiltration capacity. The *CN* value is mainly related to the soil type and land use, and it is determined by referring to the *CN* value table in the TR-55 Manual of the U. S. Soil Protection Agency [35]. The SCS-CN formula is as follows [32]:

$$Q=\frac{(P-\lambda S)^2}{P+(1-\lambda)S}, \tag{4}$$

$$S=25.4\times\left(\frac{1000}{CN}-10\right), \tag{5}$$

where P refers to the total rainfall amount, mm; Q is the surface runoff, mm; λ is the initial rainfall-loss rate; S is the maximum water-storage capacity of the soil; and CN is a dimensionless parameter ranging from 0 to 100 [32].

2.1.2 Flood risk-assessment method for people and vehicles

Multiple reports on urban-flooding events have shown that many human-casualty and vehicle-damage incidents occur on urban roads [7,29,30]. Therefore, this study focuses on risk assessments for people and vehicles on roads exposed to inundation under different extreme rainfall and street-layout scenarios. Separate flood risk assessments were performed for adults and children. For the vehicle flood risk evaluation, the Honda Accord and Audi Q7 were selected as representative vehicles because they are common vehicle types with extensive reference information available from previous studies [7,8,14,36].

The stability-criterion parameters for different people and vehicles in flood conditions were obtained from a study by Xia et al. [36]. They proposed a formula to calculate the incipient velocity of people in floodwaters based on a force analysis for people in urban floods. They then used the toppling instability threshold to evaluate the flood hazard degree (*HD*) for people in floodwaters.

The formula for the incipient velocity of the human body during toppling instability in floodwater is [7,8,14,36]

$$U_c=\alpha\left(\frac{h}{h_p}\right)^{\beta}\sqrt{\frac{m_p}{\rho_f h^2}-\left(\frac{a_1}{h_p^2}+\frac{b_1}{hh_p}\right)(\alpha_2 m_p+b_2)}, \tag{6}$$

where U_c is the incipient flow velocity; h is the water depth; ρ_f is the water density; α and β are empirical coefficients; a_1, b_1, a_2, and b_2 are coefficients that reflect the characteristics of the human body; and h_p and m_p are the human height and weight, respectively [7,8,14,36].

Similarly, the incipient velocity formula for vehicles in floodwaters is [36]

$$U_c=\alpha\left(\frac{h}{h_c}\right)^{\beta}\sqrt{2gl_c\left[\rho_c h_c/(\rho_f h)-R_f\right]}, \tag{7}$$

$$R_f=\frac{h_c\rho_c}{\rho_f h_k}, \tag{8}$$

where ρ_c is the vehicle density; h is the water depth; l_c and h_c are the vehicle length and height, respectively; h_k is the critical water depth at which the vehicle begins to float; and α and β are empirical coefficients [7,8,14,36].

Based on the above formulas for the incipient velocities of people and vehicles, the *HD* values for people and vehicles were calculated as follows [36]:

$$HD = \min(1.0, u_f / U_c), \quad (9)$$

where u_f is the actual flow velocity of the floodwater threatening human and vehicle safety. Note that the *HD* value range is from 0 to 1. The closer the actual flow velocity is to the incipient velocity of the considered people or vehicles, the larger the *HD* value, which indicates a higher flood risk [7,14].

2.2 Simulation scenarios

2.2.1 Street-layout simulation

The characteristics of the underlying urban surface of an area become increasingly complex with ongoing urbanization. Urban microtopography is co-characterized by land type, such as street, house, or grassland. Among them, the street layout is the most important controlling factor in the context of urban flooding because the street network may act as a flood pathway under extreme rainfall [37]. The urban street layout is affected by a variety of factors, which are mainly related to the natural terrain, design objectives, and land-use types; these are planned in accordance with relevant professional standards [38,39]. To explore the hydrodynamic mechanisms and flood risk pertaining to different street layouts, four typical urban street types were selected for this study based on an investigation of current urban street layouts in China [40]. These layouts were regular grid, irregular grid, radial, and annular, and are hereafter referred as S1–S4, respectively. These four street-layout types span the main street-distribution pattern types of Chinese megacities; thus, they are representative layout types, according to previous studies [41].

The Cityengine (Cityengine 2019.0) platform was employed to produce virtual idealized street layouts based on the four typical urban street-layout types considered in this study [42]. The Cityengine platform is a comprehensive urban-planning and design tool, and it has been widely used in the development of digital cities and related fields. The unique language used for Cityengine is called computer generated architecture (CGA) [43], and high-quality 3D building models can be generated based on principles written in the CGA language.

In this study, virtual idealized urban street layouts were produced via the CGA language implemented on the Cityengine platform. The design parameters (Table 1) were determined based on the urban-planning standards of China to ensure the authenticity of the generated urban street layouts [44]. The building and road densities were used as control variables and were uniformly set to 50% and 20%, respectively. The total length and area of the urban streets were set to 43 km and 1.8 km^2, respectively. The main, secondary trunk, and branch roads constituted 40%, 30%, and 30% of the layout, respectively. In all scenarios, the bottom elevation was set to that of an ideal terrain with a slope of 3%, decreasing from northwest to southeast. In accordance with the parameter settings, four groups of 3 km × 3 km block-scale street layouts were generated using the Cityengine platform. The four street layouts and corresponding 3D images are shown in Figure 1.

2.2.2 Extreme rainfall events

Two extreme rainstorms, which occurred in Beijing on July 21, 2012 and in Zhengzhou on July 20, 2021, were utilized as representative extreme rainstorms that caused considerable losses and significantly impacted China in recent years [14]. These rainstorms were labeled BJ 721 and ZZ 720, respectively. Then, the main rainfall processes of these two extreme rainstorms were selected as rainfall scenarios to implement simulations under extreme rainstorm conditions. The selected rainfall durations of BJ 721 and ZZ 720 were 16 and 24 h, respectively, and the total rainfall amounts were 212.5 and 605.2 mm, respectively. The observed rainfall processes of BJ 721 and ZZ 720 are shown in Figure 2.

2.3 Numerical model set-up

Numerical models of urban inundation were constructed for the four considered urban street layouts using the TELEMAC-2D module. First, elevation reconstructions of the urban street-layout data were generated using a geographic information system (ArcGIS 10.2) platform. Second, the land use of each considered area was classified according to the following three categories: buildings, roads, and green spaces. According to previous studies, the Manning coefficients of these three land-use types are 0.2, 0.05, and 0.5, respectively. Moreover, the *CN* values were set to 98, 94, and 80, respectively [35,45]. The basic data preparations for the 2D hydrodynamic model are shown in Figure 3.

The basic data were pre-processed using the BlueKenue software package, and the research area was mesh-divided with a 4-m grid resolution, which yielded a total of 361201 nodes and 720000 grids. The main boundary parameter conditions were as follows: a closed boundary was set for the upstream side (west and north sides), and a free-flow boundary was set for the downstream side (east and south sides) [46]. No initial inundation was set on the surface, and the total simulation time was 36 h with a 2-s time step.

The building-runoff process was generalized as follows. During the elevation reconstruction, the area covered by buildings was raised to a given height, such that the runoff could not overflow from the building tops. Because the grid was continuous, the runoff generated by the roof could still flow to other areas. Under extreme rainstorm conditions, almost all pipe networks were in the “full operation” state, and the pipe-network function could essentially be ignored in the later period of rainfall. In this study, a particular amount

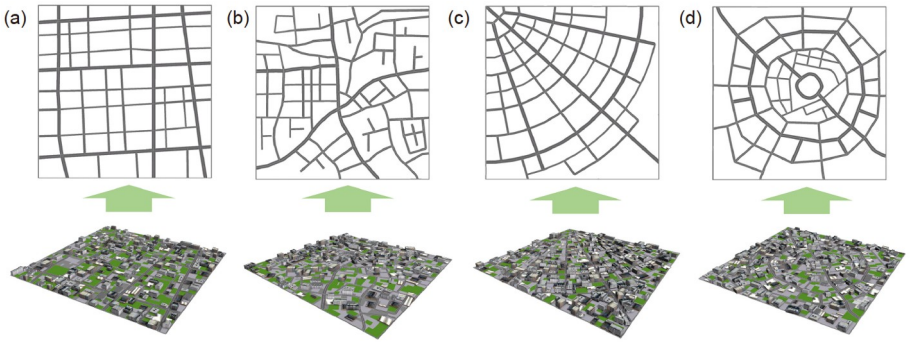

Figure 1 Planar and 3D images of designed street layouts. (a) Regular grid (S1); (b) irregular grid (S2); (c) radial (S3); (d) annular (S4).

Table 1 Main design parameters of megacity urban streets related to layouts [41]

Symbol	Parameter	Minimum value	Maximum value	General value
X1	Main-road pavement width	3.0 m	–	4.0 m
X2	Secondary trunk-road pavement width	2.5 m	–	3.5 m
X3	Branch-road pavement width	2.0 m	–	3.0 m
X4	Curb stone height	10 cm	15 cm	15 cm
X5	Main-road red line width	40 m	50 m	50 m
X6	Secondary trunk-road red line width	20 m	35 m	35 m
X7	Branch-road red line width	14 m	20 m	20 m
X8	Number of two-way lanes on main road	6	8	6
X9	Number of two-way lanes on secondary trunk road	2	4	4
X10	Number of two-way lanes on branch road	2	2	2

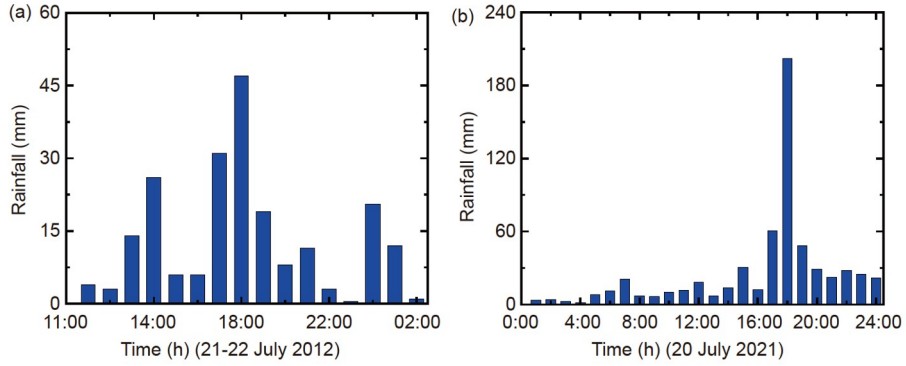

Figure 2 Observed extreme rainfall processes. (a) BJ 721; (b) ZZ 720.

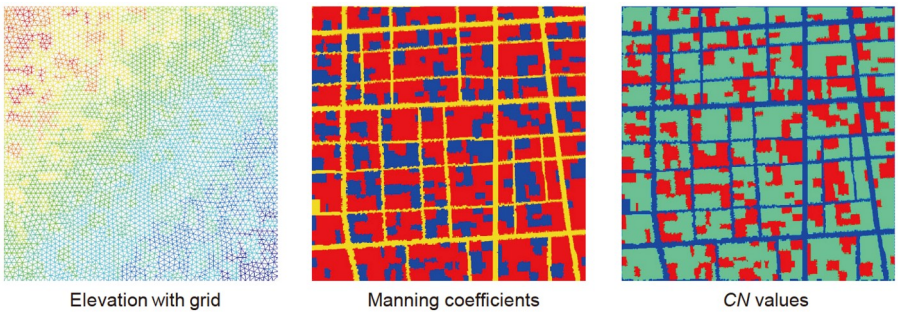

Figure 3 Basic data preparations for 2D hydrodynamic model (taking S1 as an example).

of rainfall was deducted from the rainfall input to generalize the drainage capacity of the drainage network. Based on the above settings, 2D hydrodynamic inundation models of the four considered street-layout scenarios were constructed. A rationality analysis of the scenario-simulation results revealed that the runoff coefficients and runoff processes of the constructed models were reasonable and could satisfy the requirements of the numerical experiments performed in this study.

3 Results

3.1 Street-inundation simulation results for different scenarios

3.1.1 Statistical analysis of inundation variables

The peak value of the inundated area (PVIA) refers to the inundated area at the time of the maximum flood volume. Here, the PVIA values for water depths exceeding 15, 30, and 50 cm, that is, $PVIA_{15}$, $PVIA_{30}$, and $PVIA_{50}$, respectively, were determined for each of the considered scenarios. The results are listed in Table 2.

For ZZ 720, the highest $PVIA_{15}$ value was obtained for S4 at 3.75 km^2, which was 0.2 km^2 greater than the lowest value, which was obtained for S3, with a difference proportion of 5.3%. For the BJ 721 event, the highest $PVIA_{15}$ value was obtained for S3 at 1.68 km^2, which was 0.26 km^2 greater than the lowest value, which was obtained for S1, with a difference proportion of 15.5%. For $PVIA_{30}$ and $PVIA_{50}$, the relative orders of the values for the four street layouts differed; the highest $PVIA_{30}$ values were obtained for S4 and S3, whereas the maximum $PVIA_{50}$ values were obtained for S3 and S1, for ZZ 720 and BJ 721, respectively.

Figure 4 shows the inundation characteristic values for the different rainfall and street-layout scenarios. Figure 4(a) shows that the maximum total flood volume for ZZ 720 was obtained for S1; this value was 17.22% greater than the minimum value, which was obtained for S2. For BJ 721, the maximum and minimum total flood volumes were obtained for S4 and S2, respectively. Therefore, the S2 street layout had the smallest total flood volume for both extreme rainfall scenarios.

The water depth, particularly the street-water depth, is an important factor in flood risk evaluation. To analyze the flooding severity for the different street layouts, the maximum street-water depth values were considered; the statistical results are presented in Figure 4(b). The maximum street-water depth results were in the following order: S2 > S1 > S3 > S4 and S3 > S4 > S1 > S2 for ZZ 720 and BJ 721, respectively; the differences between the maximum and minimum values were 33.42% and 60.25%, respectively.

Higher-velocity flood flow typically creates a higher risk for people and vehicles. The maximum street-flow velocities were determined, as shown in Figure 4(c). The results were in the following order: S2 > S3 > S1 > S4 and S3 > S4 > S1 > S2 for ZZ 720 and BJ 721, respectively; the highest maximum flow velocities were 4.84 and 2.47 m/s, respectively.

Thus, the analysis of the total flood volume, maximum street-water depth, and maximum street-flow velocity performed in this study revealed that the street layout has an important impact on the inundation variables.

3.1.2 Inundation-variable change processes

This section describes the analysis of the inundation-variable change processes for the different rainfall and street-layout scenarios. The change processes of the total flood volume, total inundated area, average water depth, and average flow velocity are shown in Figure 5.

Figure 5(a) and (e) show that the rising stages of the total flood-volume change processes were similar for all four street layouts. The differences were mostly observed for the peak values and descending stages; that is, the total flood-volume peak values for S2 and S3 were clearly lower than those for S1 and S4. These differences also led to significant differences in the descent stage. Figure 5(b) and (f) show no notable differences in the total inundated-area change processes for the different layouts. Figure 5(c) and (g) show the average water-depth change processes for the different rainfall and street-layout scenarios; the variable characteristics were consistent with those of Figure 5(a) and (e). Figure 5(d) and (h) show that the average flow-velocity change processes had complex variation features with no clear change rules; overall, S3 and S4 had the highest and lowest average flow velocities, respectively.

3.1.3 Spatial distributions of maximum water depth and maximum flow velocity

Figure 6(a) shows that similar maximum street-water depth spatial distributions were obtained for the two extreme rainfall scenarios. That is, the largest maximum water-depth values were mainly distributed in the southeastern region; however, the specific distributions differed between the four street layouts. The main reason for this pattern is that the study-area elevation decreased from the northwest and southeast, and the runoff generated by the rainfall accumulated along the streets to the southeast. As shown in Figure 6(a), more areas with serious inundation (colored red) were obtained for S1. Higher maximum street-water depths (exceeding 0.5 m) were obtained for the main streets of S3. The above results indicate that the street layout has an important influence on the maximum street-water depth distribution in an extreme rainstorm scenario.

Figure 6(b) shows the maximum street-flow velocity distributions for the various conditions. Significant differences in the spatial-distribution characteristics of the maximum street-flow velocity were obtained for the different extreme

Table 2 Peak values of inundated areas (PVIAs) for water depths exceeding 15, 30, and 50 cm (km^2)

Street layout	$PVIA_{15}$		$PVIA_{30}$		$PVIA_{50}$	
	BJ 721	ZZ 720	BJ 721	ZZ 720	BJ 721	ZZ 720
S1	1.42	3.70	0.53	2.45	0.40	1.25
S2	1.63	3.61	0.42	2.50	0.21	1.32
S3	1.68	3.55	0.68	2.34	0.28	1.38
S4	1.64	3.75	0.54	2.61	0.32	1.34

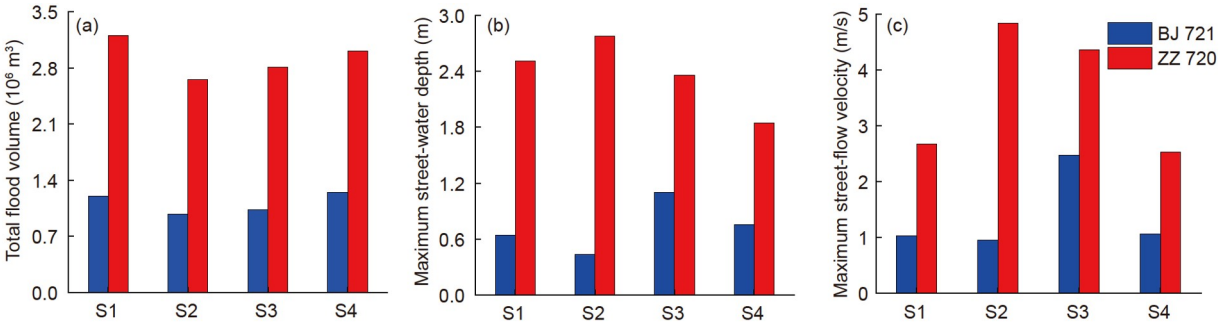

Figure 4 Inundation characteristic values for different rainfall and street-layout scenarios. (a) Total flood volume; (b) maximum street-water depth; (c) maximum street-flow velocity.

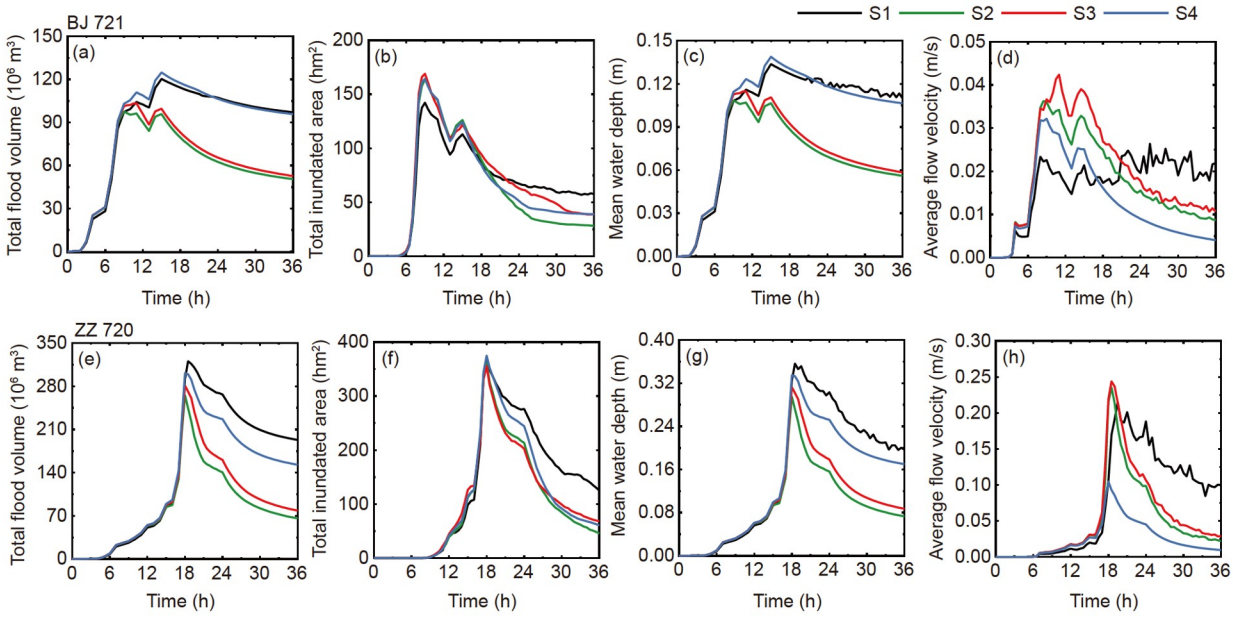

Figure 5 Change processes of (a), (e) total flood volume, (b), (f) total inundated area, (c), (g) average water depth, and (d), (h) average flow velocity.

rainfall events. Most notably, the S4 street-flow velocity was the lowest overall for both extreme rainstorms. This indicates that the S4 street layout is conducive to the drainage dispersion of waterlogging caused by extreme rainfall instead of the formation of serious flooding. For S3, the maximum street-flow velocity was mainly concentrated on the trunk road from the northwest to the southeast of the longitudinal region. This result indicates that a trunk road may become a main channel for flood discharge under extreme rainstorms with the combined effect of terrain and microtopography factors. Hence, a flood with high water depth and velocity can form, which is a serious threat to people and vehicles. As shown in Figure 6(b), the maximum street-flow velocity-distribution maps of S1 and S2 reveal that the high flow-velocity areas were mainly concentrated in the downstream main roads, road intersections, and street corners. These maps also show that complex factors, such as micro-topography and street orientation, significantly influence the

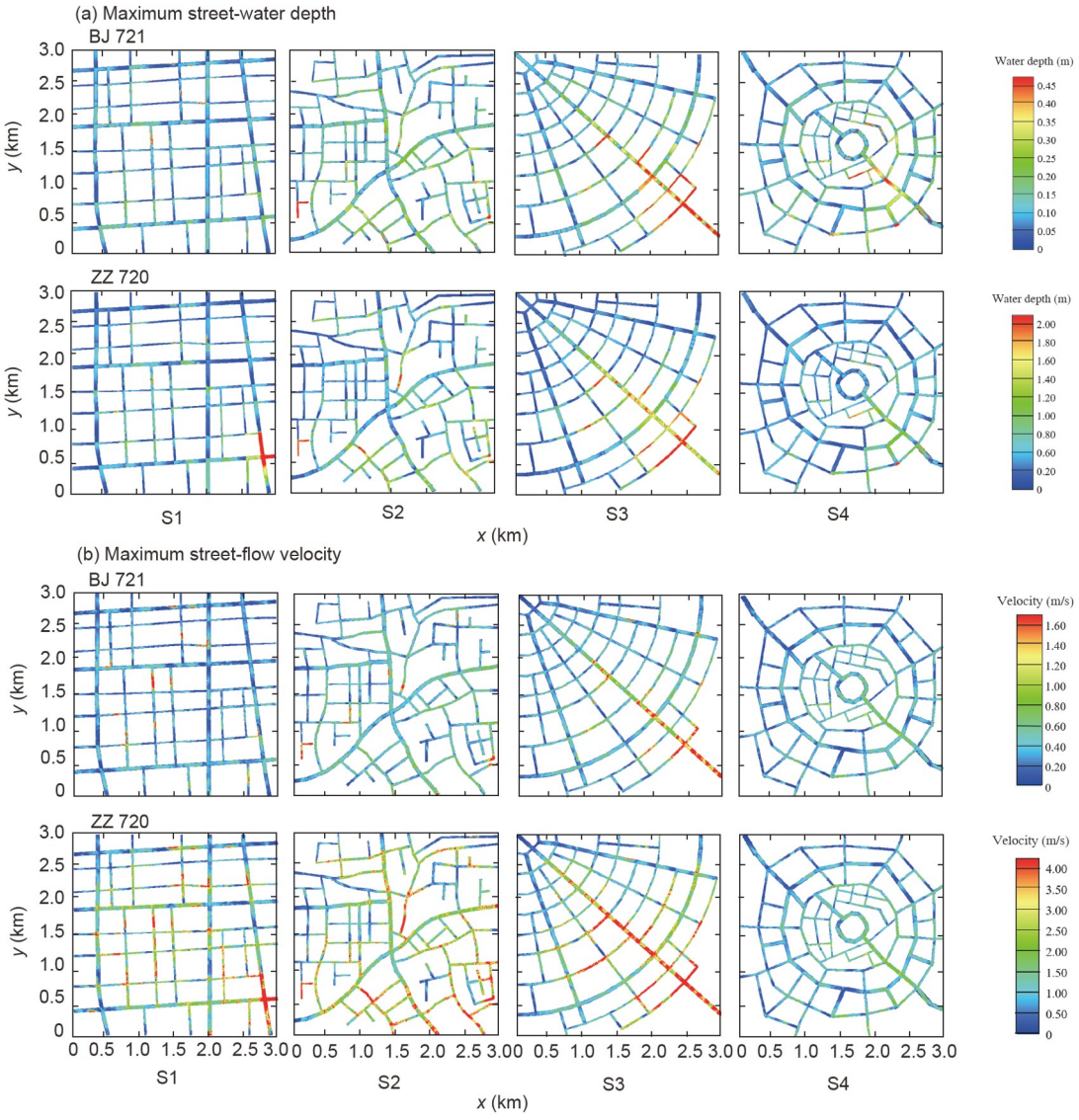

Figure 6 (a) Maximum street-water depth and (b) maximum street-flow velocity distributions for different rainfall and street-layout scenarios.

flood-flow pattern and velocity. Moreover, different street layouts correspond to different microtopography characteristics. Therefore, further analysis of the influence mechanism of the street layout on flood formation is necessary.

3.2 Flood risk assessment for people and vehicles

3.2.1 Flood risk for people

Figure 7 illustrates the maximum *HD* distributions for adults and children for the different rainfall events and street layouts considered in this study. The spatial distributions were similar for the two rainfall scenarios, and the *HD* values for children were not significantly higher than those for adults. For both adults and children, high flood-risk areas mainly occurred at exits and main roads in the study areas. Moreover, the higher flood-risk areas were mainly distributed at road intersections, which are related to the dense crossroads in this street scenario. Owing to the spatial-distribution features of S2, the maximum *HD* distribution was relatively uniform. However, for S3, the high-risk areas were concentrated in the downstream trunk roads, and they were more concentrated than those of the other street layouts. The risk area of S4 was the smallest, and the main-road *HD* was below 0.5 for BJ 721.

The road-length proportions with different *HD* levels under different rainfall and street-layout scenarios were statistically analyzed for adults and children; the results are shown in Figure 8. The *HD* values were grouped into five grades: 0–0.2, 0.2–0.4, 0.4–0.6, 0.6–0.8, and 0.8–1.0. For BJ 721, the *HD* proportion in the 0–0.2 range was dominant for both adults and children and exhibited little difference between the different street layouts. However, a clear difference was exhibited for S3, for which the *HD* proportion in the 0.8–1.0 range was significantly larger, at 3.68% and 5.53% for adults

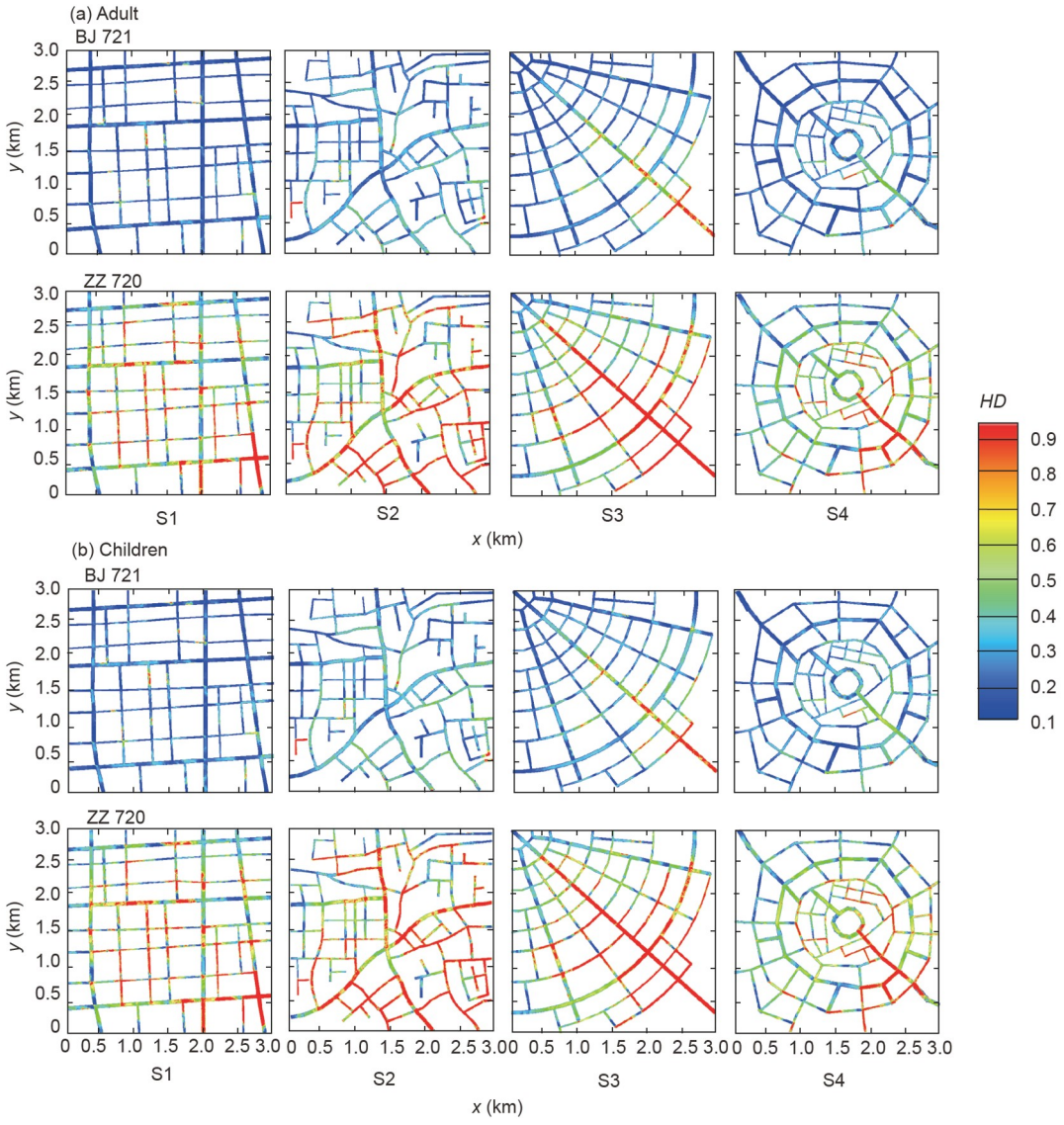

Figure 7 Maximum hazard degree (*HD*) distributions for (a) adults and (b) children for different rainfall and street-layout scenarios.

and children, respectively. For ZZ 720, the maximum *HD* proportions in the 0.8–1.0 range were obtained for S2 for both adults and children, at 35.34% and 41.86%, respectively. In contrast, the smallest *HD* proportions in the 0.8–1.0 range were obtained for S4, at 14.53% and 15.79% for adults and children, respectively. Overall, these results suggest that the street layout may have a greater impact on the *HD*-proportion distribution over the street network under heavier rainfall; however, the magnitude of this effect may vary for adults and children.

3.2.2 Flood risk for vehicles

Figure 9 illustrates the maximum *HD*-value distributions for the Honda Accord and Audi Q7 for the different rainfall events and street layouts considered in this study. Significant differences in *HD* were obtained for the different street layouts; however, no clear differences were observed in the results for the two vehicle types. The distribution characteristics also revealed that the high-*HD* areas were mainly concentrated in the downstream regions, main roads, and corners. Further quantitative analysis is required to determine the quantitative differences of the specific *HD* values.

The road-length proportions with different *HD* ranges for vehicles were determined for the different rainfall and street-layout scenarios considered in this study, and Figure 10 shows the results. For BJ 721, few differences were observed in the grade structure for the different rainfall and street-layout scenarios for both the Honda Accord and Audi Q7. Moreover, the proportion in the 0–0.2 range exceeded 90% in all cases. However, for BJ 721, the greatest *HD* proportion in the 0.8–1.0 range was obtained for the Audi Q7 and S2, at 5.82%. For ZZ 720, the maximum *HD* proportion in the 0.8–1.0 range was obtained for S2 and the Honda Accord, at 28.60%. For the Audi Q7, the largest *HD* proportion in the

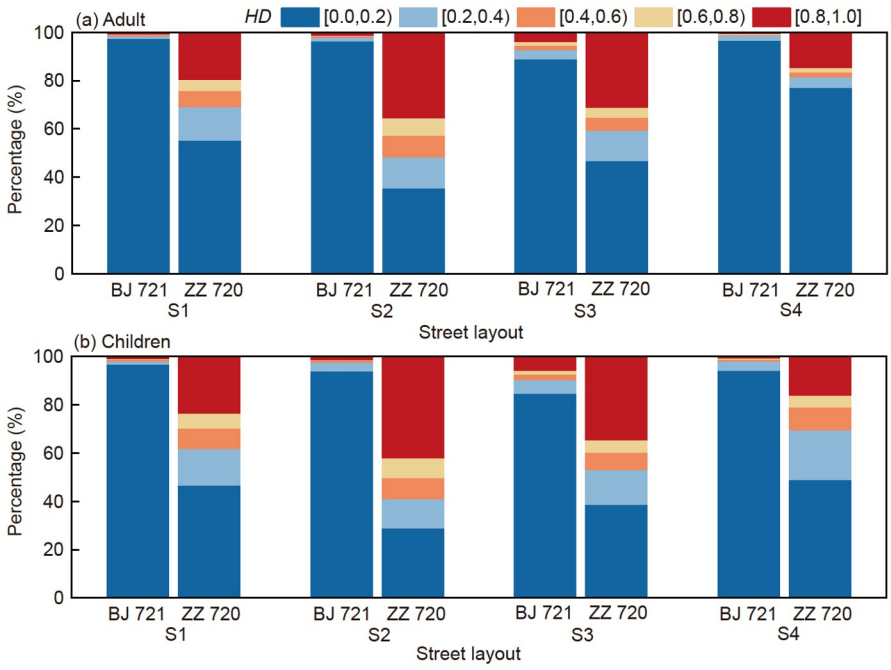

Figure 8 *HD* proportions for (a) adults and (b) children for different rainfall and street-layout scenarios.

0.8–1.0 range was obtained for S3 and ZZ 720, at 27.12%. For ZZ 720, the smallest *HD* proportions in the 0.8–1.0 range for the Honda Accord and Audi Q7 were obtained for S4, at 12.78% and 12.68%, respectively. Overall, for the same rainfall event and street layout, the road-length proportion with high-range *HD* values for vehicles are generally smaller than those for people.

4 Discussion

4.1 Influence mechanism of urban street layout on inundation

Urban forms, which primarily include street layouts, building coverage, and microtopographies, have considerable influence on the formation process and inundation characteristics of urban flooding, as confirmed by many studies [8,21,22]. Previous studies have mainly differed in terms of their research methods, the spatial variables of the urban forms, and the statistical-representation variables of the urban floods. This study focused on the impact of street layout on urban flood risk and obtained meaningful findings that are useful for analyzing the influence mechanism of urban street layout on inundation.

The main methods employed in this field are laboratory experiments, numerical simulation, and their combination; numerical simulation is the more popular method owing to its advantage of situational flexibility [47,48]. The building spatial distribution, obstacle or building coverage, street layout, and slope are most selected parameters used to characterize the synthetic urban forms of these simulations. The typical variables used to characterize urban flooding are the total flood volume, flow velocity, water depth, outflow discharge, and Froude number [24]. In the present study, numerical simulations that focused on the street-layout spatial characteristics were conducted. The street layout was the dominant factor when generating the underlying urban surface, and four street-distribution types were selected: regular grid, irregular grid, radial, and annular. The building-area proportion and road length were consistent for all four scenarios, and the building distribution was determined according to the street layout. The selected urban-inundation variables included the flood volume, flow velocity, and water depth. The influence of the street layout on the simulated urban flooding was mainly reflected by the results of risk elevations for people and vehicles under different scenarios

From the perspective of water balance, the total flood volume should theoretically be completely consistent under a particular amount of rainfall for a consistent slope and underlying surface permeability. However, the results of this study are not consistent with this theoretical conclusion. The results show that the change processes and statistical results for the key inundation variables differed for the various street-layout scenarios. For different street layouts, the floodwater spatial distributions were affected by different floodwater paths; this generated differences in confluence times and, thus, different flood curves. Different water depths and velocities were obtained in specific areas, such as streets and corners, which yielded different risk levels. This behavior has also been confirmed by Li et al. [22] and Bruwier et al. [21]. However, owing to the differences in the urban forms among the different street layouts, the surface-

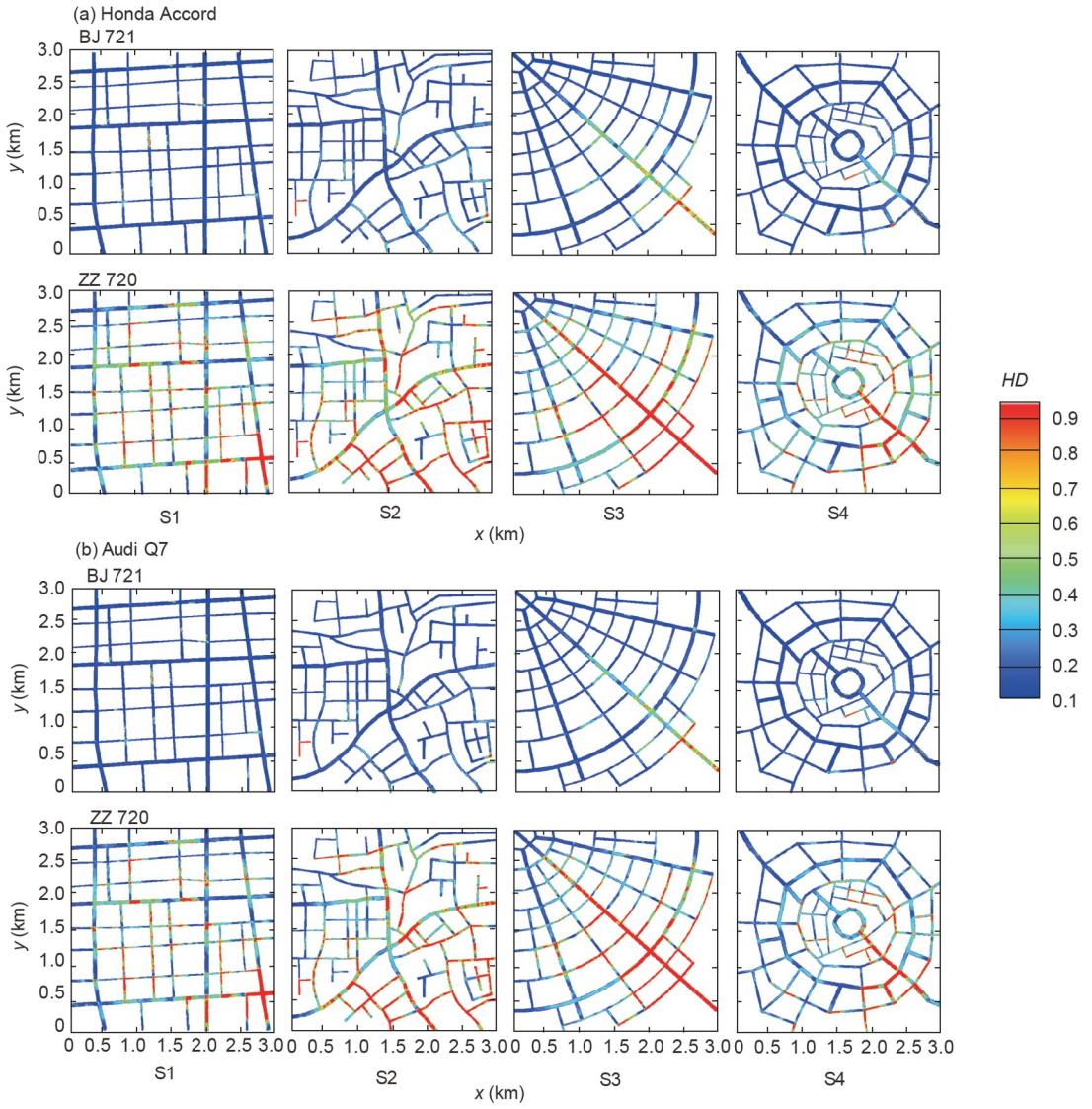

Figure 9 Maximum *HD* distributions of (a) Honda Accord and (b) Audi Q7 vehicles for different rainfall and street layout scenarios.

inundation flow paths varied when they gathered towards drainage outlets. Therefore, different durations were obtained, which yielded different peak values and lag times for the flooding processes. This analysis further indicates that urban streets typically act as floodwater paths under extreme rainstorm conditions and their distributions affect the flood-formation process; this is also a key finding and innovation of this study. Furthermore, the street-layout influence mechanism is relevant because the floodwater paths vary under the different influence mechanisms that arise from variations in the urban form, which is dominated by urban buildings. Further in-depth studies and comparative analysis of this aspect are needed.

The flow regimes are also affected by the micro-topographies formed by different urban street layouts. Under the effects of local topography and spatial geometric characteristics, the flow velocity typically increases at points with abrupt terrain changes, and the Froude number changes significantly. Additionally, the flood changes from slow to turbulence flow, and high-water depths or flow velocities can easily form in small areas. This phenomenon has been explored in previous studies [21]. In particular, Mignot et al. [24] observed that the Froude number of a flood involving obstacles is closely related to the obstacle locations. The present study also determined that higher flow velocities can form more easily at road intersections and corners, which may be owing to the disturbance to the flood-flow process caused by these obstacles as well as the sudden change in the flow regime. Further in-depth studies on the street-layout influence mechanism on the flood process and flood formation will aid scientific application of the above laws. In addition, optimized urban-road planning based on these findings would better support water-sensitive urban design and aid the construction of more livable cities.

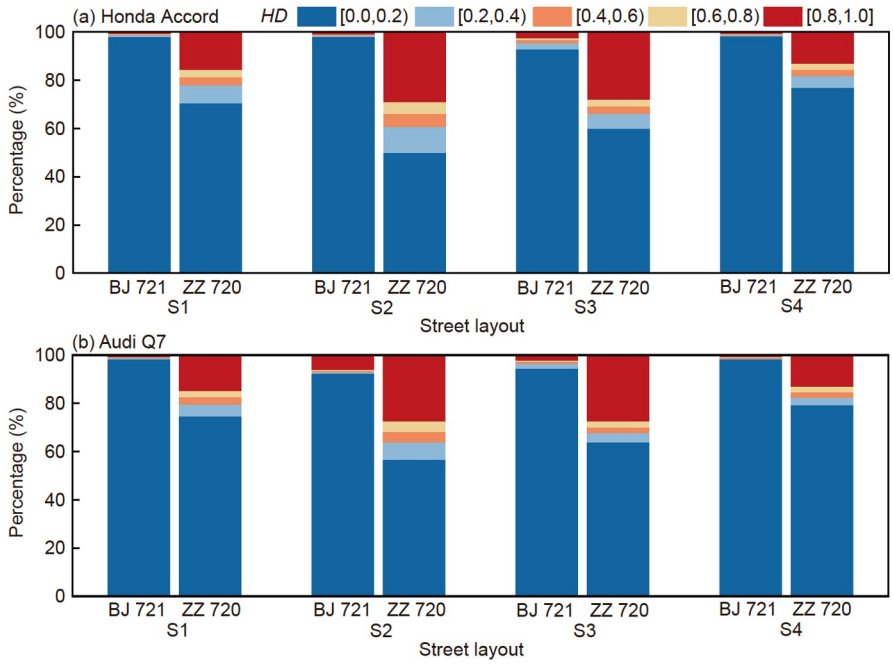

Figure 10 (a) Honda Accord and (b) Audi Q7 *HD* proportions for different rainfall and street-layout scenarios.

4.2 Inspiration for flood-sensitive urban planning and block-scale design

The underlying urban surface is a natural-synthetic landform formed by human activities and artificial structures based on natural terrain. After urbanization, the rainfall-runoff process has completely different characteristics from those of the natural state. In the context of urban flooding, the flow path and inundation distribution are mainly affected by urban microtopography, which is itself impacted by the relevant urban forms, particularly the street layout [49]. By combining the findings of the present study with those of relevant previous studies, inspiration for flood-sensitive urban planning and block-scale design can be obtained.

In the context of urban planning, flood-sensitivity analysis under different schemes should be performed with consideration to different urban forms and street layouts [25,27,50]. Comprehensive urban development and street-layout planning schemes may be proposed through flood risk analysis under different scenarios. Such schemes should combine sponge city construction, low-impact development, and the implementation of best management practices [51,52]. For example, this study showed that the annular layout yielded a significantly smaller maximum water depth, peak flow, and flow velocity as well as minimal flood risk to people and vehicles compared with those of other street layouts. Therefore, annular-type street layouts are preferable from a planning perspective, with the premise of meeting functional requirements. Some forward-looking explorations have been performed based on this. For example, Yang et al. [31] proposed an integrated building-information modeling computational engine approach to infrastructure-vulnerability assessment related to a stormwater drainage-building-road transport nexus in the context of urban flooding; their approach yielded an innovative tool for urban planning.

Model construction and scenario simulation may be used to better identify flood-prone and high-risk areas and streets for urban flood management [53]. In cases where high flood risk to people and vehicles are identified, street-based prevention measures may be prepared in advance. For intersections prone to water accumulation, manholes and warning signs may provide risk warnings to people and vehicles [31].

4.3 Limitations and uncertainties of this study

This study had some limitations and uncertainties. A limited number of street-layout scenarios were analyzed. Moreover, virtual scenarios were considered, for which the complex underlying surfaces were idealized and simplified; these may be important sources of uncertainty. Therefore, when discussing the results of this study, the limited and simplified street-layout scenarios should be noted. In addition, virtual urban street-layout scenarios were considered; therefore, no measured urban rainfall-runoff data were available to verify the model calibration. The parameters were set based on parameters and building-model experience derived from actual study areas in the past and were used for scenario simulation after reasonable analysis; however, some parameter uncertainties may exist. However, the method was appropriate for the purposes of this study. That is, regularity cognition was achieved through comparison of the results obtained for different scenarios. Because the same set of

parameters was used for all models, the general trends in the findings were robust to some extent.

Finally, the scale effect was another source of uncertainty in this study. Numerical experiments were performed on the block scale with a research area of 3 km × 3 km. Thus, the general trends identified in this work may be inapplicable to a large-scale area. Overall, whether the conclusions of this study are applicable to the overall urban scale is unclear, and the influence of the scale effect should also be considered when discussing the general trends of the urban inundation simulation results. Further studies are required to analyze the general trends and scale effects of urban inundation on various spatial scales.

5 Conclusions

With the changing environment, urban flood disasters caused by extreme rainfall are occurring more frequently and greatly threatening the sustainable development of cities. People and vehicles are most at risk when urban flood disasters occur in cities. From the perspective of the urban rainfall-runoff process, urban inundation is deeply impacted by the underlying urban surface. The urban street layout is an important influencing factor for the urban form. Therefore, exploration of the impact of street layout on urban flood risk to people and vehicles under extreme rainfall is important. In this study, numerical experiments were performed to construct four typical street-layout scenarios on the block scale. A risk-analysis method was implemented based on human-vehicle instability; hence, the impact of street layout on urban flood risk was investigated. The main findings are as follows.

(1) The simulation results confirmed that the street layout has a considerable effect on the spatial distributions of the key inundation variables, such as the maximum water depth and maximum water velocity, as well as the flood-volume and inundated-area change processes under extreme rainfall on the block scale. Under the same extreme rainfall scenario, the greatest differences in the total flood volume, maximum street-water depth, and maximum street-flow velocity values obtained for the different street layouts were 17.22%, 60.25%, and 61.50%, respectively.

(2) Statistical analysis of the simulation results revealed that the flood risk to people and vehicles are mainly reflected in the flood-risk spatial distributions and proportion structures, especially the highest and lowest risk grades. Overall, the irregular-grid street layout had the highest proportion of high-risk sections. That is, the high-risk sections for adults and children comprised 35.34% and 41.86% of the total, respectively, and those for the Honda Accord and Audi Q7 (as representative vehicles) occupied 28.60% and 27.12% of the total, respectively.

(3) Among the four street layouts considered in this study, the annular street layout had the best performance in terms of urban-inundation characteristics and risk levels. That is, under the same rainfall condition, the lowest flood severity and smallest high-grade risk proportions were obtained for that layout. For the same extreme rainfall scenario, the proportions of high-risk road sections for adults and children were 58.89% and 62.28% smaller than those for the highest-scoring layout, and those for the Honda Accord and Audi Q7 were 55.31% and 53.04% smaller than those for the highest-scoring layout, respectively.

From the perspective of block-scale urban planning and design, the results of this study confirmed the impact of urban street layout on urban inundation and quantified the impact of street layout on the flood risk to people and vehicles. The overall conclusions drawn from the street-layout scenarios designed in this study were robust under both extreme rainfall events. The findings of this study have implications for "flood-sensitive" street layouts on the block scale.

Owing to the complexity of urban hydrodynamic processes, this study had the following limitations. In particular, scale effects must be considered; that is, whether the conclusions of this study can be applied to different spatial scales is unclear. In addition, uncertainties were introduced by the limited extreme rainfall and street-layout scenarios as well as the model simulation uncertainties, which must be further studied in future research.

This work was supported by the National Natural Science Foundation of China (Grant Nos. 52009139 & 51739011), the National Key R&D Program of China (Grant No. 2022YFC3090600), and Open Fund of Beijing Key Laboratory of Urban Water Cycle and Sponge City Technology, Beijing Normal University (Grant No. HYD2022OF02).

1 Agonafir C, Pabon A R, Lakhankar T, et al. Understanding New York City street flooding through 311 complaints. J Hydrol, 2022, 605: 127300
2 He J, Qiang Y, Luo H, et al. A stress test of urban system flooding upon extreme rainstorms in Hong Kong. J Hydrol, 2021, 597: 125713
3 Luo P, Luo M, Li F, et al. Urban flood numerical simulation: Research, methods and future perspectives. Environ Model Software, 2022, 156: 105478
4 Cheng X T, Liu C J, Li C Z, et al. Evolution characteristics of flood risk under changing environment and strategy of urban resilience improvement (in Chinese). J Hydraul Eng, 2022, 53: 757–768, 778
5 Zhang H, Zhang J, Fang H, et al. Urban flooding response to rainstorm scenarios under different return period types. Sustain Cities Soc, 2022, 87: 104184
6 Zhou Q, Leng G, Su J, et al. Comparison of urbanization and climate change impacts on urban flood volumes: Importance of urban planning and drainage adaptation. Sci Total Environ, 2019, 658: 24–33
7 Dong B, Xia J, Zhou M, et al. Integrated modeling of 2D urban surface and 1D sewer hydrodynamic processes and flood risk assessment of people and vehicles. Sci Total Environ, 2022, 827: 154098
8 Dong B, Xia J, Zhou M, et al. Experimental and numerical model studies on flash flood inundation processes over a typical urban street. Adv Water Resources, 2021, 147: 103824
9 Bernardini G, Romano G, Soldini L, et al. How urban layout and

pedestrian evacuation behaviours can influence flood risk assessment in riverine historic built environments. Sustain Cities Soc, 2021, 70: 102876
10 Singh P, Sinha V S P, Vijhani A, et al. Vulnerability assessment of urban road network from urban flood. Int J Disaster Risk Reduction, 2018, 28: 237–250
11 EL Bilali A, Taleb I, Nafii A, et al. A practical probabilistic approach for simulating life loss in an urban area associated with a dam-break flood. Int J Disaster Risk Reduction, 2022, 76: 103011
12 Cai Y J, Cheng H Y, Wu S F, et al. Breaches of the Baige Barrier Lake: Emergency response and dam breach flood. Sci China Tech Sci, 2020, 63: 1164–1176
13 Wang H, Zhou J, Tang Y, et al. Flood economic assessment of structural measure based on integrated flood risk management: A case study in Beijing. J Environ Manage, 2021, 280: 111701
14 Dong B, Xia J, Li Q, et al. Risk assessment for people and vehicles in an extreme urban flood: Case study of the "7.20" flood event in Zhengzhou, China. Int J Disaster Risk Reduction, 2022, 80: 103205
15 Joo S, Ogawa Y, Sekimoto Y. Road-reconstruction after multi-locational flooding in multi-agent deep RL with the consideration of human mobility - Case study: Western Japan flooding in 2018. Int J Disaster Risk Reduction, 2022, 70: 102780
16 Han Z Y, Long D, Han P F, et al. An improved modeling of precipitation phase and snow in the Lancang River Basin in Southwest China. Sci China Tech Sci, 2021, 64: 1513–1527
17 Papilloud T, Keiler M. Vulnerability patterns of road network to extreme floods based on accessibility measures. Transp Res Part D-Transp Environ, 2021, 100: 103045
18 Borowska-Stefańska M, Kowalski M, Wiśniewski S, et al. The impact of self-evacuation from flood hazard areas on the equilibrium of the road transport. Saf Sci, 2023, 157: 105934
19 Li Z J, Liu J H, Mei C, et al. Comparative analysis of building representations in telemac-2d for flood inundation in idealized urban districts. Water, 2019, 11: 1840
20 Huang C L, Hsu N S, Liu H J, et al. Optimization of low impact development layout designs for megacity flood mitigation. J Hydrol, 2018, 564: 542–558
21 Bruwier M, Maravat C, Mustafa A, et al. Influence of urban forms on surface flow in urban pluvial flooding. J Hydrol, 2020, 582: 124493
22 Li X, Erpicum S, Mignot E, et al. Influence of urban forms on long-duration urban flooding: Laboratory experiments and computational analysis. J Hydrol, 2021, 603: 127034
23 Wang Y, Li C, Liu M, et al. Spatial characteristics and driving factors of urban flooding in Chinese megacities. J Hydrol, 2022, 613: 128464
24 Mignot E, Camusson L, Riviere N. Measuring the flow intrusion towards building areas during urban floods: Impact of the obstacles located in the streets and on the facade. J Hydrol, 2020, 583: 124607
25 Lu X, Shun Chan F K, Chen W Q, et al. An overview of flood-induced transport disruptions on urban streets and roads in Chinese megacities: Lessons and future agendas. J Environ Manage, 2022, 321: 115991
26 Zhou S, Liu Z, Wang M, et al. Impacts of building configurations on urban stormwater management at a block scale using XGBoost. Sustain Cities Soc, 2022, 87: 104235
27 Choi Y, Kang J, Kim J. Urban flood adaptation planning for local governments: Hydrology analysis and optimization. Int J Disaster Risk Reduction, 2021, 59: 102213
28 Yi Y J, Xu W Q, Liu H X. Reestablish of flood disaster chronology and analysis of the flood control standard in Xiong'an New Area. Sci Sin Tech, 2022, 52: 1543–1554
29 Lazzarin T, Viero D P, Molinari D, et al. Flood damage functions based on a single physics- and data-based impact parameter that jointly accounts for water depth and velocity. J Hydrol, 2022, 607: 127485
30 Wang N, Hou J, Du Y, et al. A dynamic, convenient and accurate method for assessing the flood risk of people and vehicle. Sci Total Environ, 2021, 797: 149036
31 Yang Y, Ng S T, Dao J, et al. BIM-GIS-DCEs enabled vulnerability assessment of interdependent infrastructures – A case of stormwater drainage-building-road transport Nexus in urban flooding. Automation Construction, 2021, 125: 103626
32 Kaveh K, Bui M D, Rutschmann P. Integration of artificial neural networks into TELEMAC-MASCARET system, new concepts for hydromorphodynamic modeling. Adv Eng Software, 2019, 132: 18–28
33 Moulinec C, Denis C, Pham C T, et al. TELEMAC: An efficient hydrodynamics suite for massively parallel architectures. Comput Fluids, 2011, 51: 30–34
34 Anh L N, Tran D D, Thong N, et al. Drastic variations in estuarine morphodynamics in Southern Vietnam: Investigating riverbed sand mining impact through hydrodynamic modelling and field controls. J Hydrol, 2022, 608: 127572
35 United States Department of Agriculture. Urban Hydrology for Small Watersheds. Technical Release 55 (TR-55). 2nd ed. Washington: USDA, 1986
36 Xia J, Falconer R A, Wang Y, et al. New criterion for the stability of a human body in floodwaters. J Hydraulic Res, 2014, 52: 93–104
37 Ferrari A, Viero D P. Floodwater pathways in urban areas: A method to compute porosity fields for anisotropic subgrid models in differential form. J Hydrol, 2020, 589: 125193
38 Standard for urban residential area planning and design (in Chinese). GB 50180-2018. Beijing: China Architecture & Building Press, 2018
39 Standard for urban comprehensive transport system planning (in Chinese). GB/T 51328-2018. Beijing: China Architecture & Building Press, 2018
40 Yang D D, Han Y Q, Cao L, et al. Research of urban community road system layout optimization strategy based on simulation analysis of generation and concentration (in Chinese). Landsc Archit, 2019, 26: 101–106
41 Liu J H, Shi H Y, Mei C, et al. Effect of urban subsurface spatial pattern on community-scale flooding processes via numerical simulation (in Chinese). Adv Water Sci, 2022, 33: 881–893
42 Koziatek O, Dragićević S. iCity 3D: A geosimualtion method and tool for three-dimensional modeling of vertical urban development. Landscape Urban Planning, 2017, 167: 356–367
43 Yuan T, Deng F, Li T S. Fusion method of real topographic and virtual simulation model based on CGA rules. J Geoma, 2021, 46: 216–220
44 Code for design of urban road engineering. CJJ 37—2012. Beijing: China Architecture & Building Press, 2016
45 Mei C, Liu J H, Wang H, et al. Urban flood inundation and damage assessment based on numerical simulations of design rainstorms with different characteristics. Sci China Tech Sci, 2020, 63: 2292–2304
46 Bruwier M, Mustafa A, Aliaga D G, et al. Influence of urban pattern on inundation flow in floodplains of lowland rivers. Sci Total Environ, 2018, 622-623: 446–458
47 Mignot E, Dewals B. Hydraulic modelling of inland urban flooding: Recent advances. J Hydrol, 2022, 609: 127763
48 Xia J Q, Dong B L, Li Q J, et al. Study on hydrodynamic mechanisms and disaster reduction countermeasures of recent urban floods (in Chinese). China Flood Drought Manage, 2022, 32: 66–71
49 Zhu M, Li H, Sze N N, et al. Exploring the impacts of street layout on the frequency of pedestrian crashes: A micro-level study. J Saf Res, 2022, 81: 91–100
50 Sharifi A. Resilient urban forms: A review of literature on streets and street networks. Building Environ, 2019, 147: 171–187
51 Zellner M, Massey D, Minor E, et al. Exploring the effects of green infrastructure placement on neighborhood-level flooding via spatially explicit simulations. Comput Environ Urban Syst, 2016, 59: 116–128
52 Cheng T, Huang B, Yang Z, et al. On the effects of flood reduction for green and grey sponge city measures and their synergistic relationship —Case study in Jinan sponge city pilot area. Urban Clim, 2022, 42: 101058
53 Yuan F, Xu Y, Li Q, et al. Spatio-temporal graph convolutional networks for road network inundation status prediction during urban flooding. Comput Environ Urban Syst, 2022, 97: 101870